4-2015

Direct observation of the recovery of an antiferroelectric phase during polarization reversal of an induced ferroelectric phase

Hanzheng Guo
Iowa State University

Xiaoli Tan
Iowa State University, xtan@iastate.edu

Direct observation of the recovery of an antiferroelectric phase during polarization reversal of an induced ferroelectric phase

Abstract

Electric fields are generally known to favor the ferroelectric polar state over the antiferroelectric nonpolar state for their Coulomb interactions with dipoles in the crystal. In this paper, we directly image an electric-fieldassisted ferroelectric-to-antiferroelectric phase transition during polarization reversal of the ferroelectric phase in polycrystalline Pb0.99{Nb0.02[(Zr0.57Sn0.43)0.92Ti0.08]0.98}O3.With the electric-field in situ transmission electron microscopy technique, such an unlikely phenomenon is verified to occur by both domain morphology change and electron-diffraction analysis. The slower kinetics of the phase transition, compared with ferroelectric polarization reversal, is suggested to contribute to this unusual behavior.

Disciplines

Ceramic Materials | Other Materials Science and Engineering | Semiconductor and Optical Materials

Comments

This article is from *Physical Review B* 91 (2015): 1, doi:10.1103/PhysRevB.91.144104. Posted with permission.

Direct observation of the recovery of an antiferroelectric phase during polarization reversal of an induced ferroelectric phase

Hanzheng Guo and Xiaoli Tan*

Department of Materials Science and Engineering, Iowa State University, Ames, Iowa 50011, USA

(Received 12 January 2015; revised manuscript received 30 March 2015; published 10 April 2015)

Electric fields are generally known to favor the ferroelectric polar state over the antiferroelectric nonpolar state for their Coulomb interactions with dipoles in the crystal. In this paper, we directly image an electric-field-assisted ferroelectric-to-antiferroelectric phase transition during polarization reversal of the ferroelectric phase in polycrystalline $Pb_{0.99}\{Nb_{0.02}[(Zr_{0.57}Sn_{0.43})_{0.92}Ti_{0.08}]_{0.98}\}O_3$. With the electric-field *in situ* transmission electron microscopy technique, such an unlikely phenomenon is verified to occur by both domain morphology change and electron-diffraction analysis. The slower kinetics of the phase transition, compared with ferroelectric polarization reversal, is suggested to contribute to this unusual behavior.

DOI: 10.1103/PhysRevB.91.144104 PACS number(s): 77.80.−e, 81.30.Hd, 61.05.jm, 77.84.Cg

It is generally believed that electric dipoles will be aligned to the applied electric-field direction either in a liquid or a gaseous phase. A similar phenomenon has been observed in the ferroelectric (FE) and antiferroelectric (AFE) solid-state crystals where electric dipoles are parallel to each other in a FE phase and antiparallel in an AFE phase [1,2]. It has been experimentally shown that an electric field favors the FE phase over the AFE phase by forcing the antiparallel dipoles being switched to along the external field direction, leading to a first-order AFE-to-FE phase transition [3,4]. In the most studied AFE compositions that are chemically modified from the prototype $PbZrO_3$, the electric-field-triggered AFE-to-FE phase transition is generally manifested by the development of a large polarization as well as a significant volume expansion when the applied field reaches a critical value [4–6]. Microscopically, the nanoscale feature of incommensurate modulations in the AFE state transforms into large ferroelectric domains, accompanied with the disappearance of the characteristic satellite diffraction spots [7,8].

Other external stimuli, such as mechanical stresses, are also known to influence or even trigger the transition between the AFE and the FE phases [9–14]. It has been generalized that a symmetric external stimulus (i.e., hydrostatic pressure) stabilizes the AFE phase, whereas an asymmetric stimulus (i.e., electric field) only favors the FE phase in Sn- and Ti-modified $PbZrO_3$-based ceramics [15]. However, our recent investigation based on *in situ* x-ray-diffraction and macroscopic strain measurements has unambiguously demonstrated that it is possible for an electric field to induce an AFE phase out of a FE phase by appropriately choosing the chemical composition and manipulating the electric-field application process [6]. Such a FE-to-AFE phase transition is manifested by the volume stain reduction as well as the reappearance of AFE x-ray-diffraction peaks when the polarity of the applied field is reversed [6]. Further verification of such an unusual phenomenon has been revealed in a $NaNbO_3$-based lead-free ceramic with a finely tuned composition at the AFE/FE phase boundary where a comparable free-energy profile of both phases is present, presumably the prerequisite condition for the recovery of the AFE phase upon electric reversal [16].

In the present paper, the unlikely electric field-assisted FE-to-AFE transition is directly visualized via microstructure imaging. A $PbZrO_3$-based ceramic is employed for the demonstration due to its finely tuned composition located at the AFE/FE phase boundary as well as the distinct microstructural features between the AFE and the FE states. Employing the electric-field *in situ* transmission electron microscopy (TEM) technique [17–21], the domain morphologies and their corresponding electron-diffraction patterns are simultaneously monitored during the electric loading and reversal process.

The polycrystalline $Pb_{0.99}\{Nb_{0.02}[(Zr_{0.57}Sn_{0.43})_{0.92}Ti_{0.08}]_{0.98}\}O_3$ (PNZST 43/8.0/2) ceramic was synthesized using the solid-state reaction method. Details can be found in our previous report [22]. X-ray diffraction was used to ensure phase purity of the sintered pellet. Dielectric properties were measured at 1 kHz with an LCZ meter (Keithley 3322) during heating and cooling at a rate of 3 °C/min. The first two cycles of polarization vs electric-field hysteresis loops were recorded with a standardized ferroelectric test system (RT66A, Radiant Technologies) at room temperature and 4 Hz. For the electric-field *in situ* TEM experiments, disk specimens (3 mm in diameter) were prepared from as-processed pellets through standard procedures including grinding, cutting, dimpling, and ion milling. The dimpled disks were annealed at 200 °C for 2 h to minimize the residual stresses before Ar-ion milling to the point of electron transparency. *In situ* TEM experiments were carried out on a Phillips CM30 microscope operated at 200 kV. Experimental details are similar to those reported in Refs. [17–21].

The PNZST 43/8.0/2 ceramic is found to be at the AFE/FE phase boundary at room temperature [23,24]. Due to the thermal hysteresis of the first-order AFE-FE phase transition, either the AFE or the FE phase can be dominant in the ceramic at room temperature depending on thermal history [22]. This is experimentally verified by the dielectric properties measured during heating and successive cooling, shown in Fig. 1(a). The anomalies at ∼43 °C during heating and at ∼−8 °C during cooling define the thermal hysteresis of the first-order AFE-FE transition [22]. The result indicates that at room temperature (25 °C), the ceramic is in the AFE state when cooled from sintering or annealing and is in the FE state when warmed up from low temperatures (−100 °C). The AFE and FE phases are hence energetically comparable at room temperature in

*Corresponding author: xtan@iastate.edu

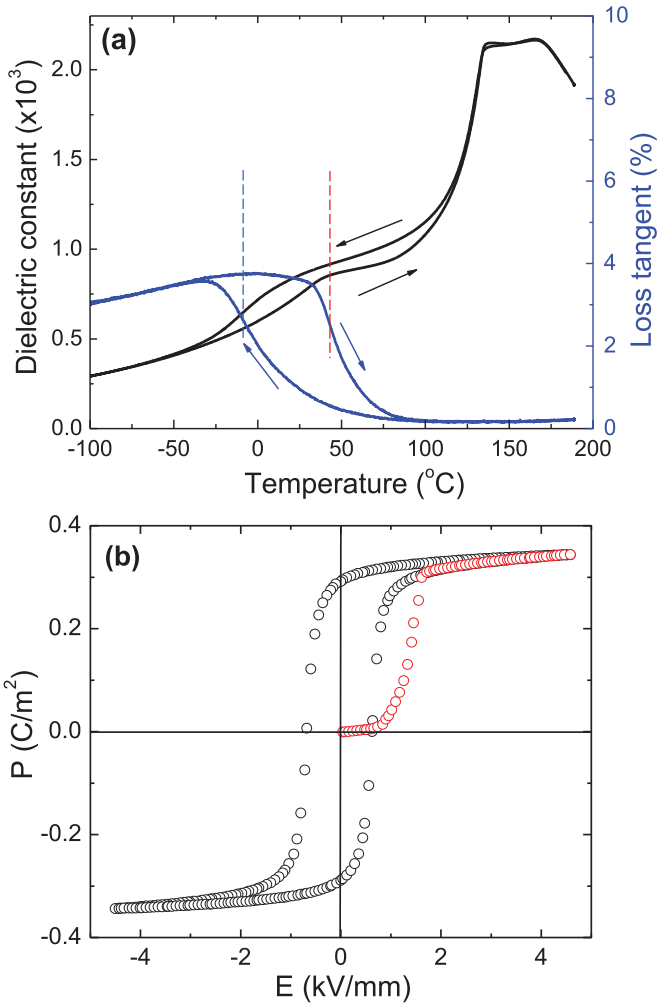

FIG. 1. (Color online) (a) Dielectric properties of a bulk polycrystalline PNZST 43/8.0/2 specimen measured at 1 kHz and 3 °C/min during heating and cooling. The anomalies at −8 °C and 43 °C are indicated by the dashed vertical lines. (b) The first two cycles of the polarization (P) vs electric field (E) hysteresis loops from a bulk polycrystalline PNZST 43/8.0/2 specimen measured at room temperature and 4 Hz. The data points in red are from the first quarter cycle of the applied field.

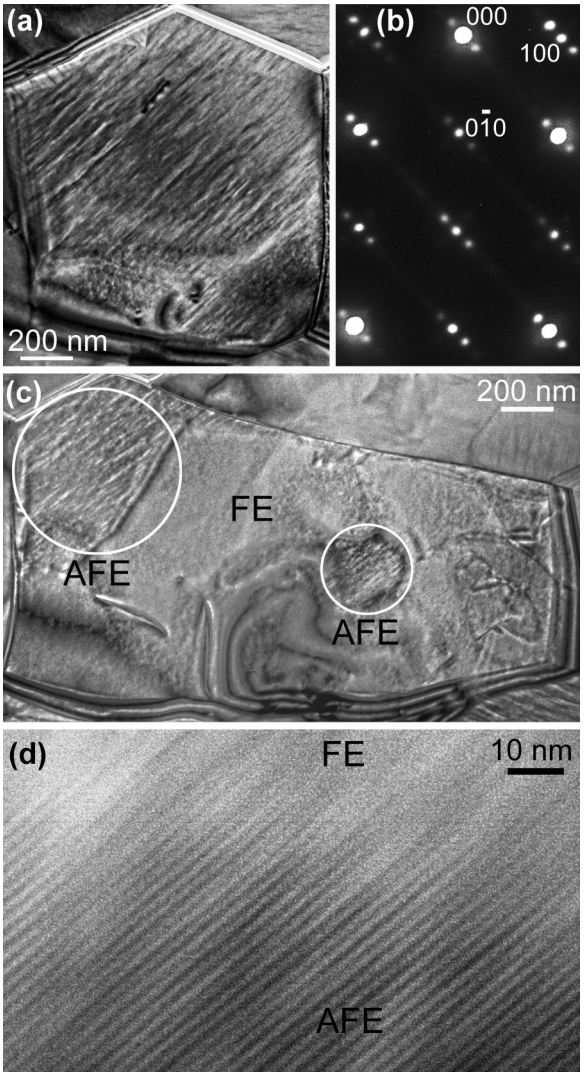

FIG. 2. Typical microstructures of the polycrystalline PNZST 43/8.0/2 recorded under the [001] zone axis. (a) TEM bright field micrograph of a grain of the AFE phase, (b) its corresponding electron-diffraction pattern, (c) a grain with mixed FE and AFE phases, and (d) a close examination of the AFE/FE interface.

this composition, which is believed to be essential for the electric-field-assisted FE-to-AFE phase transition to occur [6,16].

The behavior shown in Fig. 1(a) for the PNZST 43/8.0/2 ceramic is verified by an irreversible AFE-to-FE phase transition at room temperature when the electric field is applied to the virgin AFE ceramic [6,24]. The induced FE phase remains upon removal of the applied field as shown in Fig. 1(b). The critical electric field that triggers the AFE-to-FE phase transition is determined to be 1.2 kV/mm during the first quarter cycle of the electric field (highlighted in red). The large polarization developed in the induced ferroelectric phase is largely preserved in the second quarter cycle when the applied field is unloaded. A normal ferroelectriclike behavior is observed during the subsequent electric loading, manifested by the square-shaped loop with a large remanent polarization of 0.29 C/m^2 at a frequency of 4 Hz. It should be noted that the polarization loop remains square shaped without apparent pinches even at a frequency as low as 10 mHz at room temperature.

Microstructure analysis of the PNZST 43/8.0/2 ceramic supports the macroscopic property measurements depicted in Fig. 1. In the virgin state of PNZST 43/8.0/2, TEM examination reveals that most grains are predominantly in the AFE phase [Fig. 2(a)]. The characteristic incommensurate modulation is seen to occupy most of the grain. The corresponding satellite diffraction spots, aligning along the ⟨110⟩ direction [7,8], are present in the [001] zone-axis selected area electron-diffraction pattern [Fig. 2(b)]. A few large grains in the TEM specimen display mixed AFE and FE phases and grains occupied primarily by the FE phase are occasionally noticed. Figure 2(c) shows such a large grain with the coexisting AFE (in the circled region) and FE (the rest part of the grain) phases. In contrast to the AFE phase, the FE phase

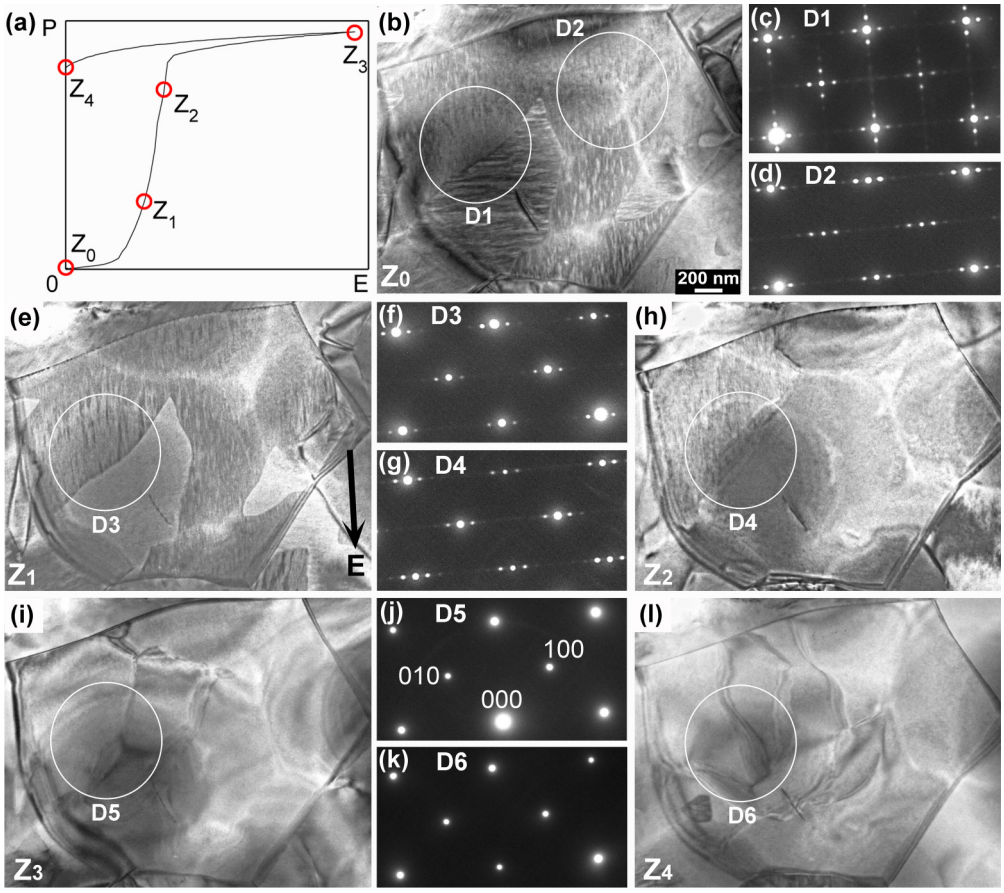

FIG. 3. (Color online) Electric-field-induced AFE-to-FE phase transition in polycrystalline PNZST 43/8.0/2. (a) Replotted P vs E loop in Fig. 1(b) for the part in the first quadrant. The red open circles on the curve, marked as Z_0–Z_4, correspond to the applied field levels where bright field images and electron-diffraction patterns are recorded during the *in situ* TEM experiment. (b), (e), (h), (i), and (l) Bright field micrographs of a [001]-oriented grain at electric fields corresponding to Z_0–Z_4, respectively. The magnification marker in (b) is applicable to other micrographs as well. The dark arrow in (e) indicates the direction of the applied fields. (c), (d), (f), (g), (j), and (k) [001] zone-axis electron-diffraction patterns recorded from selected areas marked by the bright circles as D1–D6, respectively. The indexing of the diffraction spot is exemplified in (j).

is nearly featureless with no modulation fringes and no satellite diffraction spots. The AFE/FE interphase interface appears to be diffuse [Fig. 2(d)]. For the AFE phase, close-up examination reveals clearly the incommensurate modulation strips along the $\{110\}$ planes, which is consistent with previous reports [7,25].

The switching between the AFE and the FE phases at room temperature driven by external electric fields is then directly visualized using the *in situ* TEM technique. A [001]-orientated grain in its virgin AFE state is focused as shown in Figs. 3 and 4. To assist the understanding of the electric-field application sequence during the *in situ* TEM experiment, the polarization (P) vs electric-field hysteresis loop for the first cycle on a separate bulk ceramic specimen is included.

Figure 3 displays the result for the AFE-to-FE phase transition from the virgin AFE state under applied electric fields, which correspond to Z_0–Z_4 on the partial hysteresis loop in the first quadrant shown in Fig. 3(a). In the virgin state (corresponding to Z_0 on the hysteresis loop), the grain of interest is occupied by 90° AFE domains with orthogonally oriented textures in contrast [Fig. 3(b)]. Electron-diffraction patterns recorded from regions D1 and D2 are displayed in Figs. 3(c) and 3(d). Region D1 covers two AFE domains, and two sets of satellite diffraction spots are seen. Region D2 is within a large AFE domain, and hence only one set of satellite spots is present. The result is consistent with our previous studies on a similar composition [7].

When an electric field corresponding to the point of Z_1 is applied to the virgin state specimen, dramatic changes are observed. All the AFE domains with horizontal textures become featureless as shown in Fig. 3(e). Region D3, the same as D1 in Fig. 3(b), produces only one set of satellite diffraction spots [Fig. 3(f)]. Apparently those featureless domains are now in the FE state, and the rest of the grain remains in the AFE state. Comparing Fig. 3(e) with Fig. 3(b), the following observations are apparent regarding the electric-field-induced AFE-to-FE phase transition in this grain. First, the transition shows an orientation dependence of AFE 90° domains, taking place first in domains with horizontal textures. Second, the transition preserves the positions of the original interfaces. However, it should be made clear that the original interfaces are charge neutral 90° AFE domain walls whereas after transition they become FE/AFE interphase interfaces. Presumably these interfaces between a polar and a nonpolar phase are not charge neutral.

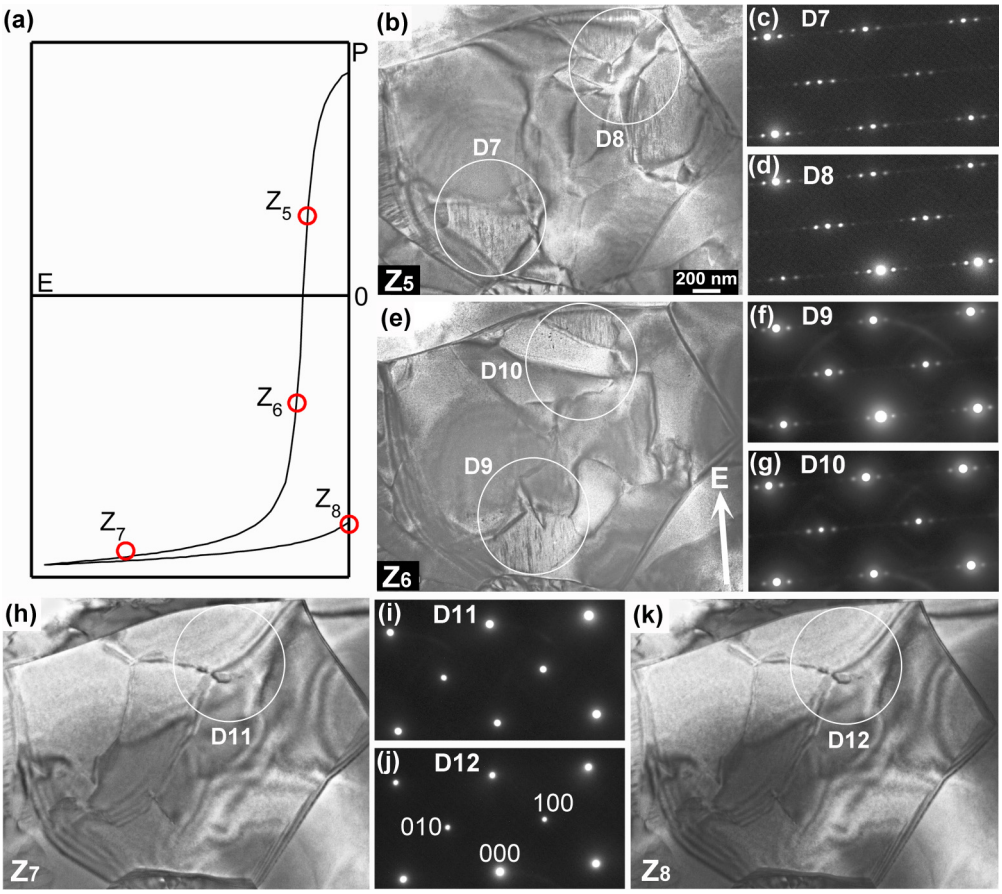

FIG. 4. (Color online) Direct visualization of the recovery of the AFE phase during polarization reversal of the induced FE phase in the same [001]-oriented grain as in Fig. 3. (a) Replotted P vs E loop in Fig. 1(b) for the part in the second and the third quadrants. The red open circles on the curve, marked as Z_5–Z_8, correspond to the applied field levels where bright field images and electron-diffraction patterns are recorded during the *in situ* TEM experiment. (b), (e), (h), and (k) Bright field micrographs of the grain at electric fields corresponding to Z_5–Z_8, respectively. The magnification marker in (b) is applicable to other micrographs as well. The bright arrow in (e) indicates the direction of the applied fields. (c), (d), (f), (g), (i), and (j) [001] zone-axis electron-diffraction patterns recorded from selected areas marked by the bright circles as D7–D12, respectively. The indexing of the diffraction spot is exemplified in (j).

Further electric-field-induced AFE-to-FE phase transition proceeds gradually in this [001]-orientated grain. In Fig. 3(h), only the left corner of the grain is still in the AFE state. At the maximum applied field, corresponding to Z_3, the AFE-to-FE transition is complete in this grain, demonstrated by the disappearance of the textured contrast [Fig. 3(i)] and the satellite diffraction spots [Fig. 3(j)]. Consistent with the results shown in Fig. 1 from bulk specimens, the *in situ* TEM study confirms that the induced FE phase is metastable at room temperature in this composition. After the electric field is removed (corresponding to Z_4), none of the satellite diffraction spots reappear [Fig. 3(k)], and the bright field contrast of this grain remains largely unchanged from the FE state [Fig. 3(l)].

In classic ferroelectric compounds, such as $BaTiO_3$ and $PbTiO_3$, the polarization reversal is thought to take place through the nucleation and growth of new domains with opposite polar vectors upon field reversal [26,27]. For the polycrystalline PNZST 43/8.0/2, the polarization vs electric-field loop shown in Fig. 1(b) seems to suggest a normal polarization reversal behavior of the induced FE phase. It is supposed to stay as the FE phase all the time during the polarization reversal. However, our previous electrostrain and *in situ* x-ray-diffraction measurements on bulk specimens revealed hidden phase transitions during polarization reversal [6]. These hidden transitions are directly visualized with the *in situ* TEM technique.

Figure 4(a) displays the partial hysteresis loop in the second and the third quadrants in order to assist the understanding of the field application sequence during the *in situ* TEM experiment. When the electric field reverses its polarity and reaches the value corresponding to Z_5, the same [001]-oriented grain exhibits a surprising recovery of the AFE phase: Three regions with vertical textures form in the grain [Fig. 4(b)]. The reappearance of satellite diffraction spots verifies that these regions are of AFE nature [Figs. 4(c) and 4(d)]. It is interesting to note several observations pertinent with such an unusual phase transition. First, all three regions of the recovered AFE phase are at the grain boundaries, suggesting the formation of a nonpolar AFE phase out of a polar FE phase has to overcome a lower-energy barrier in grain boundary regions. The high concentration of charged defects at the grain boundaries can reduce the energy associated with the depolarization field whereas the mechanical strain exerted from surrounding grains may favor the AFE phase which is slightly more compact in

volume. Second, all the three regions of the recovered AFE phase in this grain have vertical textures. The AFE domain with vertical textures transforms after those with horizontal textures to the FE phase during the initial loading [Figs. 3(e) and 3(h)]. So this set of AFE domains in this grain is more stable under the current electric and mechanical conditions. Third, the region of the recovered AFE phase in the lower left part of the grain displays textures orthogonal to those in the virgin state.

The recovered AFE phase is observed only within a very narrow electric-field range during the TEM study. A slight increase in the magnitude of the electric field in the reverse direction to Z_6 leads to the disappearance of the recovered AFE phase in the region of the right, reduction in size of the AFE region in the top, and a shift in position of the one in the lower part of the grain [Fig. 4(e)]. Further increases in the electric-field magnitude completely eliminate the recovered AFE phase, and the whole grain becomes FE phase [Figs. 4(h) and 4(i)]. Presumably the FE phase shown in Fig. 4(h) has polarizations opposite to the FE phase displayed in Fig. 3(i). Again the induced FE phase is metastable and is observed to persist after the applied electric field is removed [Figs. 4(j) and 4(k)].

Our *in situ* TEM study, therefore, directly visualizes the complex process of the microstructure in a ceramic with a phase boundary composition in response to electric fields with a reversed polarity. The polarization reversal of the induced FE phase is mediated by a transient AFE phase and is accomplished through two successive phase transitions, first from FE to AFE and then from AFE to FE with reversed polarization. Most importantly, the results demonstrate that an electric field can disrupt the long-range dipole order in a FE phase and produce a nonpolar AFE phase. These hidden phase transitions are overlooked by the macroscopic polarization measurement because the coercive field for polarization reversal and the critical fields for phase transitions are almost of the same value in these $PbZrO_3$-based AFE/FE phase boundary compositions [6,24]. In contrast, the coercive field is greater than the critical field for the FE to AFE transition and lower than that for the AFE to FE transition in lead-free $NaNbO_3$-based AFE/FE phase boundary compositions [16]. Consequently, the polarization hysteresis loops exhibit apparent distortions and are capable of revealing the phase transitions during polarization reversal of the metastable induced FE phase.

It should be emphasized that the electric-field-assisted FE-to-AFE phase transition observed in the present paper is highly unusual. To rationalize the underlying physics of this phenomenon, the free-energy profile for a first-order phase transition is considered. According to the Landau-Devonshire phenomenological theory [28], the free-energy of the material can be expressed in a polynomial form of the polarization P: $W(P) = \alpha P^2 + \beta P^4 + \gamma P^6$ with $\alpha > 0$, $\beta < 0$, and $\gamma > 0$. Here, only the magnitude of P is considered for simplification due to the polycrystalline nature of the material. Our experimental observations suggest that the energy has local minima at both the AFE and the FE states: The one at $P = 0$ denotes the nonpolar AFE phase and the other at the spontaneous polarization of the FE phase. In a multidimensional space, the FE state exists in several equivalent polarization orientations connected by a low-energy pathway. Reversing the polarization of a FE state may take two distinct routes: (1) The material can undergo two consecutive phase transitions (FE-to-AFE and then AFE-to-FE) through the recovery of the AFE phase; (2) the material maintains the FE polar state and accomplishes the 180° polarization reversal by going through some intermediate FE polarization orientations along the low-energy pathway. Even though with different rate dependencies [16], both processes occur simultaneously in the current polycrystalline ceramic. Compared with FE polarization reversal, the phase transitions presumably show a slower kinetics and would be favored by slowly applied (or even dc) electric fields in the reversed direction.

On the technology side, these phase boundary compositions with hidden phase transitions during polarization reversal can be exploited for solid-state cooling devices because they are very likely to display a strong electrocaloric effect [29]. In these ceramics, the latent heat of the first-order transitions and the caloric effect from polarization alignment can be properly tuned to work in synergy, leading to much enhanced temperature change under adiabatic conditions [30].

In conclusion, with help of the electric-field *in situ* TEM technique, the transitions between the AFE and the FE phases are directly visualized in a finely tuned composition of PNZST 43/8.0/2 located at the AFE/FE phase boundary. Starting from an AFE phase in the virgin state, a metastable FE phase is induced first via the forward AFE-to-FE phase transition. It occurs in sequence in different sets of AFE domains. When the polarity of the electric field is reversed subsequently, the polarization reversal of the induced FE phase is accompanied by two successive phase transitions. The partial recovery of the AFE phase appears to start at the grain boundaries in the polycrystalline material. Even though a field-assisted FE-to-AFE transition is highly unusual, it can be rationalized by considering the free-energy landscape and the large difference in kinetics between the phase transition and the polarization reversal.

This work was supported by the National Science Foundation (NSF) through Grant No. DMR-1037898. S. E. Young is acknowledged for his assistance on ceramic fabrication and electric property measurements. TEM experiments were performed at the Ames Laboratory, which is operated for the U.S. DOE by Iowa State University under Contract No. DE-AC02-07CH11358.

[1] C. Kittel, Phys. Rev. **82**, 729 (1951).
[2] K. M. Rabe, in *Functional Metal Oxides: New Science and Novel Applications*, edited by S. B. Ogale, T. V. Venkatesan, and M. Blamire (Wiley-VCH, Weinheim, 2013), pp. 221–224.
[3] D. Viehland, D. Forst, Z. Xu, and J. F. Li, J. Am. Ceram. Soc. **78**, 2101 (1995).
[4] X. Tan, C. Ma, J. Frederick, S. Beckman, and K. G. Webber, J. Am. Ceram. Soc. **94**, 4091 (2011).
[5] P. Yang and D. A. Payne, J. Appl. Phys. **71**, 1361 (1992).
[6] X. Tan, J. Frederick, C. Ma, W. Jo, and J. Rödel, Phys. Rev. Lett. **105**, 255702 (2010).
[7] H. He and X. Tan, Phys. Rev. B **72**, 024102 (2005).

[8] H. He and X. Tan, Appl. Phys. Lett. **85**, 3187 (2004).
[9] D. H. Zeuch, S. T. Montgomery, and D. J. Holcomb, J. Mater. Res. **15**, 689 (2000).
[10] M. Avdeev, J. D. Jorgensen, S. Short, G. A. Samara, E. L. Venturini, P. Yang, and B. Morosin, Phys. Rev. B **73**, 064105 (2006).
[11] X. Tan, J. Frederick, C. Ma, E. Aulbach, M. Marsilius, W. Hong, T. Granzow, W. Jo, and J. Rödel, Phys. Rev. B **81**, 014103 (2010).
[12] D. Berlincourt, H. H. A. Krueger, and B. Jaffe, J. Phys. Chem. Solids **25**, 659 (1964).
[13] Z. Dai, Z. Xu, and X. Yao, Appl. Phys. Lett. **92**, 072904 (2008).
[14] Z. Xu, Y. J. Feng, S. G. Zheng, A. Jin, F. L. Wang, and X. Yao, J. Appl. Phys. **92**, 2663 (2002).
[15] P. Yang and D. A. Payne, J. Appl. Phys. **80**, 4001 (1996).
[16] Y. Xu, W. Hong, Y. Feng, and X. Tan, Appl. Phys. Lett. **104**, 052903 (2014).
[17] X. Tan, H. He, and J. K. Shang, J. Mater. Res. **20**, 1641 (2005).
[18] H. Guo, B. K. Voas, S. Zhang, C. Zhou, X. Ren, S. P. Beckman, and X. Tan, Phys. Rev. B **90**, 014103 (2014).
[19] C. Ma, H. Z. Guo, S. P. Beckman, and X. Tan, Phys. Rev. Lett. **109**, 107602 (2012).
[20] H. Guo, C. Zhou, X. Ren, and X. Tan, Phys. Rev. B **89**, 100104(R) (2014).
[21] X. Tan, Z. Xu, J. K. Shang, and P. Han, Appl. Phys. Lett. **77**, 1529 (2000).
[22] X. Tan, S. E. Young, Y. H. Seo, J. Y. Zhang, W. Hong, and K. G. Webber, Acta Mater. **62**, 114 (2014).
[23] H. He and X. Tan, J. Phys.: Condens. Matter **19**, 136003 (2007).
[24] J. Frederick, X. Tan, and W. Jo, J. Am. Ceram. Soc. **94**, 1149 (2011).
[25] I. MacLaren, R. Villaurrutia, B. Schaffer, L. Houben, and A. Pelaiz-Barranco, Adv. Funct. Mater. **22**, 261 (2012).
[26] W. J. Merz, Phys. Rev. **95**, 690 (1954).
[27] Y. H. Shin, I. Grinberg, I. W. Chen, and A. M. Rappe, Nature (London) **449**, 881 (2007).
[28] A. F. Devonshire, Philos. Mag. **40**, 1040 (1949).
[29] A. S. Mischenko, Q. Zhang, J. F. Scott, R. W. Whatmore, and N. D. Mathur, Science **311**, 1270 (2006).
[30] G. Schmidt, H. Arndt, G. Borchhardt, J. Cieminski, T. Petzsche, K. Borman, A. Sternberg, A. Zirnite, and V. A. Isupov, Phys. Status Solidi (a) **63**, 501 (1981).